



**VICTORIA UNIVERSITY**  
MELBOURNE AUSTRALIA

*Acute neuroinflammation promotes a metabolic shift that alters extracellular vesicle cargo in the mouse brain cortex*

This is the Published version of the following publication

Vassileff, Natasha, Spiers, Jereme G, Juliani, Juliani, Lowe, Rohan GT, Datta, Keshava K and Hill, Andrew F (2024) Acute neuroinflammation promotes a metabolic shift that alters extracellular vesicle cargo in the mouse brain cortex. *Journal of Extracellular Biology*, 3 (7). ISSN 2768-2811

The publisher's official version can be found at  
<https://isevjournals.onlinelibrary.wiley.com/doi/10.1002/jex2.165>  
Note that access to this version may require subscription.

Downloaded from VU Research Repository <https://vuir.vu.edu.au/49073/>

# Acute neuroinflammation promotes a metabolic shift that alters extracellular vesicle cargo in the mouse brain cortex

Natasha Vassileff<sup>1,2,3</sup>  | Jereme G. Spiers<sup>1,2,3</sup>  | Juliani Juliani<sup>1,4,5</sup> | Rohan G. T. Lowe<sup>6</sup> | Keshava K. Datta<sup>6</sup> | Andrew F. Hill<sup>1,7</sup> 

<sup>1</sup>The Department of Biochemistry and Chemistry, School of Agriculture, Biomedicine and Environment, La Trobe Institute for Molecular Science, La Trobe University, Bundoora, Victoria, Australia

<sup>2</sup>Clear Vision Research, Eccles Institute of Neuroscience, John Curtin School of Medical Research, College of Health and Medicine, The Australian National University, Acton, Australian Capital Territory, Australia

<sup>3</sup>School of Medicine and Psychology, College of Health and Medicine, The Australian National University, Acton, Australian Capital Territory, Australia

<sup>4</sup>Olivia Newton-John Cancer Research Institute, Heidelberg, Victoria, Australia

<sup>5</sup>School of Cancer Medicine, La Trobe University, Bundoora, Victoria, Australia

<sup>6</sup>La Trobe University Proteomics and Metabolomics Platform, La Trobe University, Bundoora, Victoria, Australia

<sup>7</sup>Institute for Health and Sport, Victoria University, Footscray, Victoria, Australia

## Correspondence

Andrew F. Hill, Institute for Health and Sport, Victoria University, Footscray, Victoria, Australia.  
Email: [Andy.Hill@vu.edu.au](mailto:Andy.Hill@vu.edu.au)

## Funding information

National Health and Medical Research Council Australia, Grant/Award Number: GNT1132604

## Abstract

Neuroinflammation is initiated through microglial activation and cytokine release which can be induced through lipopolysaccharide treatment (LPS) leading to a transcriptional cascade culminating in the differential expression of target proteins. These differentially expressed proteins can then be packaged into extracellular vesicles (EVs), a form of cellular communication, further propagating the neuroinflammatory response over long distances. Despite this, the EV proteome in the brain, following LPS treatment, has not been investigated. Brain tissue and brain derived EVs (BDEVs) isolated from the cortex of LPS-treated mice underwent thorough characterisation to meet the minimal information for studies of extracellular vesicles guidelines before undergoing mass spectrometry analysis to identify the differentially expressed proteins. Fourteen differentially expressed proteins were identified in the LPS brain tissue samples compared to the controls and 57 were identified in the BDEVs isolated from the LPS treated mice compared to the controls. This included proteins associated with the initiation of the inflammatory response, epigenetic regulation, and metabolism. These results allude to a potential link between small EV cargo and early inflammatory signalling.

## KEYWORDS

cytokines, extracellular vesicles, lipopolysaccharide, neuroinflammation, proteomics

## 1 | INTRODUCTION

Acute neuroinflammation is an inflammatory response that occurs in the central nervous system (CNS) that is characterised by the glial release of chemokines, cytokines and reactive oxygen species (ROS), which leads to further recruitment of microglia, macrophages, astrocytes and leukocytes (DiSabato et al., 2016; Norden et al., 2016). Acute inflammation occurs immediately following an insult and can be effectively recreated in vivo using lipopolysaccharide (LPS), a pathogen-associated molecular pattern (PAMP) located on the outer membrane of *Escherichia coli* (Batista et al., 2019; Zhao et al., 2019). LPS activates toll-like

Natasha Vassileff and Jereme G. Spiers contributed equally to this study.

This is an open access article under the terms of the [Creative Commons Attribution-NonCommercial-NoDerivs License](https://creativecommons.org/licenses/by-nc-nd/4.0/), which permits use and distribution in any medium, provided the original work is properly cited, the use is non-commercial and no modifications or adaptations are made.

© 2024 The Author(s). *Journal of Extracellular Biology* published by Wiley Periodicals LLC on behalf of International Society for Extracellular Vesicles.

receptor (TLR) 4, initiating a downstream cascade involving myeloid differentiation primary response protein 88 (MyD88), interleukin-1 receptor-associated kinases (IRAKs) and TNF receptor associated Factor 6 (TRAF6) (Lu et al., 2008; Zhao et al., 2019). This activation is accompanied by a change in metabolism from oxidative phosphorylation to aerobic glycolysis, in part promoted by expression of hypoxia-inducible factor-1 $\alpha$  (HIF1 $\alpha$ ) which upregulates expression of glycolytic enzymes including lactate dehydrogenase (LDH) and pyruvate dehydrogenase kinase 1 (PDK1) (Kim et al., 2006; Wang et al., 2017). The upregulation of these enzymes leads to increased lactate and pyruvate entering the tricarboxylic acid (TCA) cycle (Lauterbach et al., 2019; Meiser et al., 2016). However, in executing this pro-inflammatory state there are two prominent breaks in the TCA cycle resulting in intermediates entering the cytoplasm where they conduct regulatory functions (Geiß et al., 2022). One of these vital metabolites is citrate which stimulates lipid synthesis and the production of nicotinamide adenine dinucleotide phosphate (NADPH) and acetyl-coenzyme A (CoA), which contribute to histone acetylation, inflammatory gene transcription and fatty acid accumulation required for cell membrane expansion (Hu et al., 2016; Wang et al., 2014; Wei et al., 2016; Wellen et al., 2009). The second break is characterised by succinate accumulation which stabilizes HIF-1 $\alpha$  expression leading to sustained reprogramming through transcription, decreased mitochondrial respiration and reinforced aerobic glycolysis (Tannahill et al., 2013; Wculek et al., 2022). The regulation of gene expression culminates in the activation of transcription factors including nuclear factor kappa B subunit 1 (NF- $\kappa$ B), which leads to transcription of pro-inflammatory genes and subsequent production of pro-inflammatory cytokines including interleukins (ILs) (Lu et al., 2008). In addition to recruiting leukocytes, IL-1, IL-6 and IL-17 have been documented to regulate autophagy, a vital cellular process required for homeostasis (Ge et al., 2018).

Autophagy is a cellular process that involves the proteolytic degradation of unnecessary or dysfunctional cytosolic components through a lysosome-dependent pathway (Glick et al., 2010). Autophagy occurs constitutively under normal conditions with its up regulation occurring in response to stress which includes endoplasmic reticulum stress, mitochondrial damage and neuroinflammation (Glick et al., 2010; Wang et al., 2022). There are three main subcategories of autophagy: microautophagy, macroautophagy and chaperone-mediated autophagy (CMA). Microautophagy is characterised by the protrusion or invagination of the lysosomal or late endosomal membrane resulting in the internalisation of cytosolic proteins and organelles (Vicencio et al., 2020; Wang et al., 2022). Interestingly, there is considerable overlap between autophagy and cell-to-cell communication in the form of extracellular vesicles (EVs).

EVs are small double-lipid membraned particles, capable of traversing large distances, that are involved in intercellular communication (Colletti et al., 2021). The term EVs encompasses small EVs including exosomes, medium EVs including microvesicles, and large EVs including apoptotic bodies (Vassileff, Cheng, & Hill, 2020). The distinction between these subgroups comes down to the size of these vesicles and their biogenesis process. Small EVs are characterised as exhibiting a 50–200 nm diameter and originate from the endosomal trafficking system (Vassileff, Cheng, & Hill, 2020). They begin their biogenesis process with the maturation of early endosomes, containing material, into late endosomes (Stoorvogel et al., 1991). Cargo including proteins, RNA and lipids are transferred to the limiting membrane of what is now a multivesicular body (MVB) resulting in the formation of intra-luminal vesicles (ILVs) (Pan et al., 1985; Skotland et al., 2017). The MVB then fuses with either lysosomes, resulting in the degradation of the ILVs, or with the plasma membrane resulting in the release of small EVs (Buschow et al., 2009). Initially believed to be involved in disposal, the biogenesis of small EVs has substantial overlap with autophagy (Gudbergsson & Johnsen, 2019). Specifically, autophagosomes, involved in macroautophagy, are known to fuse with MVBs, which reduces small EV secretion (Colletti et al., 2021; Fader et al., 2008; Villarroya-Beltri et al., 2016). Furthermore, autophagy-related (ATG) proteins which are key autophagy proteins that have been shown to influence small EV biogenesis and secretion by regulating MVB acidification and therefore altering ILV formation (Gudbergsson & Johnsen, 2019; Guo et al., 2017; Murrow et al., 2015).

Despite evidence of cross talk between macroautophagy and small EV biogenesis, the stimuli for influencing communication between these pathways during neuroinflammation has not been thoroughly investigated. In this study we demonstrate that neuroinflammation influences small EV protein packaging and affects expression of TCA cycle enzymes leading to their increased presence in small EVs. This study is the first to explore the role neuroinflammation plays in the packaging of small EVs in the cortical region and uncovers how this packaging is influenced through the inter-talk between mitochondria and small EV biogenesis.

## 2 | METHODS

### 2.1 | Experimental animals and tissue collection

Ethical approval was approved by the La Trobe University Animal Ethics Committee under approval number AEC19-034 and all procedures were carried out in strict accordance with the policies and procedures outlined in the Australian Code of Practice for the Care and Use of Animals for Scientific Purposes. Wildtype C57BL/6 mice (aged 10–12 weeks) were sourced from the La Trobe Animal Research and Teaching Facility breeding colony and housed in IVC cages (3–5/cage) under standard 12-h light (lights on at 07:00) conditions with ad libitum access to food and water. On the experimental day, animals were moved to an experimental room in the same facility and administered either LPS (500  $\mu$ g/kg) or saline via i.p. injection (Biesmans et al., 2013; Dang et al.,

2019). Mice were returned to their cages for 6 h after which they were transcardially perfused with sterile saline (as detailed in [Dang et al., 2019]). The brain was then rapidly removed and the cortex isolated and frozen on powdered dry ice prior to storage at  $-80^{\circ}\text{C}$ .

## 2.2 | Pro-inflammatory mRNA expression

RNA was extracted from cortical brain tissue using a Qiagen mRNAeasy mini kit (Qiagen, Doncaster, Australia) according to the manufacturer's instructions. A total of  $1\ \mu\text{g}$  of RNA was reverse transcribed using a high capacity cDNA reverse transcriptase kit (Applied Biosystems Cat#4368813) and the expression of pro-inflammatory genes of interest (Nfkbia; Mm00477798\_m1, Nlrp3; Mm00840904\_m1, Il1 $\beta$ ; Mm00434228\_m1, Il6; Mm00446190\_m1, Tnf; Mm00443258\_m1, Ccl2; Mm01287743\_m1) was determined using Taqman Assay-on-demand kits using the geometric mean of Actb (Mm02619580\_g1) and Hprt1 (Mm03024075\_m1) as housekeeping genes. The relative expression of target genes was then calculated using the  $\Delta\Delta\text{CT}$  method relative to saline-treated control mice.

## 2.3 | Brain derived extracellular vesicle isolation from mouse cortex tissue

Brain derived EVs (BDEVs) were isolated from the cortex tissue of mice as previously described (Vassileff, Vella, Rajapaksha, et al., 2020; Vella et al., 2017). In detail, the frozen tissue was sliced on ice 2–3 mm lengthways per every 100 mg and incubated at  $37^{\circ}\text{C}$  with 800  $\mu\text{L}$  of collagenase type 3 solution (75 U/mL of collagenase (Worthington) in DPBS) per 100 mg of tissue. Ice cold inhibition solution (5 $\times$  PhosSTOP (Sigma-Aldrich), 1 $\times$  cComplete ULTRA protease inhibitor (Sigma-Aldrich), 2 mM EDTA in DPBS) was then added to the tissue to a final concentration of 1 $\times$  before resuspension and subsequent centrifugation at  $300 \times g$  at  $4^{\circ}\text{C}$  for 5 min in a standard benchtop centrifuge.

An aliquot of the  $300 \times g$  pellet, was treated with inhibition solution to a final concentration of 1 $\times$  (1 mL of 10 $\times$  inhibition solution, 9 mL of DPBS). This  $300 \times g$  pellet, which was not used for further EV isolation, was then homogenised using 18-, 21-, 25- and 27-gauge needles, sonicated at  $4^{\circ}\text{C}$  for 20 min, and centrifuged at  $10,000 \times g$  at  $4^{\circ}\text{C}$  for 5 min in a standard benchtop centrifuge, and the supernatant representative of the total brain proteome was collected.

The supernatant containing the EVs from the  $300 \times g$  spin was then further centrifuged at  $2000 \times g$  at  $4^{\circ}\text{C}$  for 10 min and  $10,000 \times g$  at  $4^{\circ}\text{C}$  for 30 min in a Type 45 Ti rotor (339160, Beckman Coulter) before being overlaid on a triple sucrose cushion consisting of Fraction 4 (F4); 1 mL of 2.5 M sucrose (20 mM 4-(2-hydroxyethyl)-1-piperazineethanesulfonic acid (HEPES) in  $\text{D}_2\text{O}$  (pH 6.4), 2.5 M protease-free sucrose, pH 7.4) with a refractive index of 1.453, followed by Fraction 3 (F3); 1 mL of 1.3 M sucrose (10.4 mL of 2.5 M sucrose, 9.6 mL of HEPES in  $\text{D}_2\text{O}$ ), with a refractive index between 1.3978 and 1.3958, followed by Fraction 2 (F2); 1 mL of 0.6 M sucrose (4.8 mL of 2.5 M sucrose, 15.2 mL of HEPES in  $\text{D}_2\text{O}$ ) with a refractive index between 1.3639 and 1.3622, in which the EVs are concentrated following ultracentrifugation indicating their density is between 1.3639 and 1.3622, followed by the supernatant from the  $10,000 \times g$  spin, in an ultra-clear thin-wall 13.2 mL tube (344059, Beckman Coulter). The gradient then underwent further centrifugation at  $200,000 \times g$  at  $4^{\circ}\text{C}$  for 180 min in a SW41 rotor (15U12301, Beckman Coulter). The entire 1 mL of each Fraction (1, 2 and 3) was subsequently collected and each was resuspended in 7 mL of ice cold DPBS prior to centrifugation at  $128,000 \times g$  at  $4^{\circ}\text{C}$  for 80 min in 26.3 mL polycarbonate centrifuge bottles (355618, Beckman Coulter) in a Type 70 Ti rotor (15U6647, Beckman Coulter). The pellets were collected and resuspended in 80  $\mu\text{L}$  of DPBS and stored at  $-80^{\circ}\text{C}$  with Fraction 2 containing the EVs.

## 2.4 | SDS-PAGE gel electrophoresis

The protein content of the brain tissue (TB) samples and BDEVs (isolated in Fraction 2) was then lysed in 1 $\times$  lysis buffer (5 M NaCl, 1 M Tris, Triton X-100, 1% (w/v) sodium deoxycholate, 1 $\times$  cComplete ULTRA protease inhibitor) at  $4^{\circ}\text{C}$  for 20 min before centrifugation at  $2500 \times g$ ,  $25^{\circ}\text{C}$  for 5 min. The protein concentration was then determined using a bicinchoninic acid (BCA) protein assay (Pierce, ThermoFisher Scientific), according to the manufacturer's instructions, and measured using the ClarioStar microplate reader (BMG Labtech). Samples were combined with LDS Sample Buffer (4 $\times$ ) (ThermoFisher Scientific NP0007), containing 5%  $\beta$ -mercaptoethanol, and incubated at  $70^{\circ}\text{C}$  for 10 min. 20  $\mu\text{g}$  of each sample was loaded onto a 4%–12% Bis-Tris Plus Gel (NuPAGE or Bolt, Invitrogen) with 1 $\times$  MES SDS running buffer (NuPAGE, Invitrogen) before undergoing transfer to a PVDF membrane and incubation with the following antibodies (EV enriched proteins: Actin, Cell Signalling 8H10D10 (MISEV category 2, 1 in 1000 dilution); Tsg101, Abcam ab83 (MISEV category 2, 1 in 500 dilution); and CD9 Abcam ab30871 (MISEV category 1, 1 in 1000 dilution); and EV non-enriched proteins: Calnexin, Abcam ab22595 (MISEV category 4, 1 in 10,000 dilution); and Nucleoporin, BD Bioscience 610497 (MISEV category 3, 1 in 1000 dilution) in 2.5% skim milk in PBS-T (0.05% Tween) (Kowal et al., 2016; Perez-Hernandez et al., 2018). The membranes were then incubated with either a mouse IgG HRP

(BioStrategy NA931) or rabbit IgG HRP (BioStrategy NA934) secondary antibody (1 in 10,000 dilution) in 2.5% skim milk in PBS-T prior to development with the Clarity ECL reagent (Bio-Rad), imaging with the ChemiDoc Touch imaging system (Bio-Rad) and analysis using Image Lab 5.2.1 (Bio-Rad).

## 2.5 | Nanoparticle tracking analysis

Size and concentration of the isolated vesicles was determined using nanoparticle tracking analysis (NTA). The samples were diluted 1 in 1000 in DPBS prior to infusion via a 1 mL syringe into the ZetaView Quatt PMX-420 (Particle Metrix). Recordings were created by scanning 30 frames per position at 11 positions with the following parameters maximum particle size: 1000, minimum particle size 10, minimum brightness 25, focus: autofocus, sensitivity: 80.0, shutter: 100 and cell temperature: 25°C. The in-built ZetaView software 8.05.14-SP7 was used for analysis of these recordings.

## 2.6 | Transmission electron microscopy

Size and morphology of the isolated vesicles was achieved using transmission electron microscopy (TEM). The formvar-copper coated grid was glow discharged for 60 s, after which 5 µL of sample was added to the grid (ProSciTech) followed by addition of 5 µL of Uranyl acetate (Agar Scientific), twice. The grid was then imaged using the JEM-2100 transmission electron microscope (Jeol).

## 2.7 | Protein digest and peptide desalting

Four control brain tissue (TB) and four LPS TB samples along with three control BDEV and three LPS BDEV samples, all of which consisted of 50 µg in 100 µL, underwent proteomic analysis. Denaturation of proteins was achieved through reconstitution of the samples in urea (8 M urea, 25 mM Tris-HCl, pH 8.0). Disulphide bonds were reduced with a 60-min incubation with TCEP (tris-2-carboxyethyl-phosphine) at a final concentration of 2 mM. Alkylation of reduced thiols was achieved through a 45-min incubation in the dark with iodoacetamine to a final concentration of 38 mM. The samples were then diluted to a final concentration of 2 M urea using 20 mM Tris-HCl. Sequencing grade trypsin (Promega) was added in a 1:50 ratio (enzyme:protein) and incubated overnight at 37°C. The peptides were desalted using StageTips according to a previously published protocol (Rappsilber et al., 2007) and dried in a speedvac.

## 2.8 | LC-MS analysis of peptides

Label-free LC-MS was performed on a Thermo Fisher Scientific Q Exactive HF mass spectrometer interfaced with a Thermo Ultimate 3000 RSLCnano UHPLC system. Reconstitution of peptides was achieved in 0.1% (v/v) trifluoroacetic acid (TFA) and 2% (v/v) acetonitrile (ACN). Peptides (500 ng) were loaded onto a PepMap C18 5 µm 1 cm trapping cartridge (Thermo-Fisher Scientific, Waltham, MA, USA) at 14 µL/min for 6 min and washed for 6 min before switching the pre-column in line with the analytical column (nanoEase M/Z Peptide BEH C18 Column, 1.7 µm, 130 Å and 75 µm ID × 25 cm, Waters). Peptides were separated at 250 nL/min using a linear ACN gradient of buffer A (0.1% (v/v) formic acid, 2% (v/v) ACN) and buffer B (0.1% (v/v) formic acid, 80% (v/v) ACN). Buffer B was increased from 12% to 30% over 54 min, then to 50% over 10 min and finally to 95% over 6 min. The column was then cleaned for 4 min in 95% buffer B and equilibrated with 2% buffer B for 10 min.

Mass spectrometry data were collected in data dependent acquisition mode. MS1 scans were acquired in the profile mode using 350–1500 m/z as MS scan range at a resolution of 60,000. The AGC target was set to  $3 \times 10^6$  while the maximum ion injection time was 30 ms. Peptide fragmentation was achieved using HCD with a normalized collision energy of 28. MS/MS spectra were collected using a TopN method with a loop count of 7 at a resolution of 60,000. The minimum AGC target for the MS2 scans was  $1.2 \times 10^4$  while maximum ion injection time was 110 ms. MS2 scans were acquired in the centroid mode.

## 2.9 | Database search

Raw files were searched using the SequestHT search engine in the Thermo Proteome Discoverer software suite (version 2.4). Searches were carried out against the *Mus musculus* UniProt reference proteome database (UP000000589, March 2021) and a decoy database containing reversed sequences with the following parameters: precursor tolerance of 15 ppm and fragment tolerance of 0.05 Da, permission of two missed trypsin cleavages, included static modification of carbamidomethyl of C, and dynamic

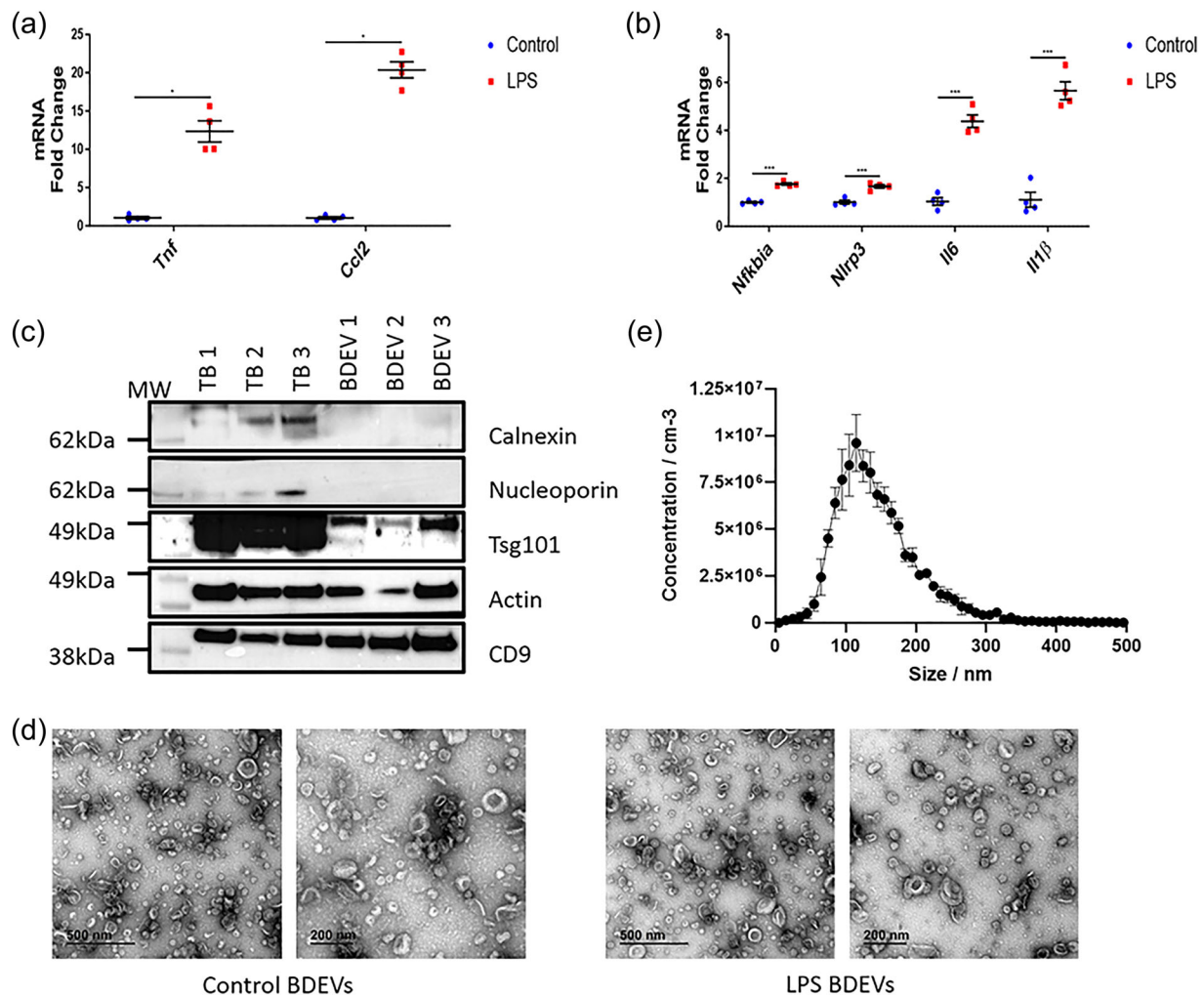


**FIGURE 1** Characterisation of model and BDEVs. Brain tissue and BDEVs isolated from the cortex of mice treated with LPS or Saline exhibit an inflammatory response and characteristics consistent with that of small EVs, respectively. (a) Brain tissue from LPS treated mice exhibited increased expression of cytokines. Mann–Whitney test,  $n = 4$ , mean  $\pm$  SEM. (b) Brain tissue from LPS treated mice demonstrated increased expression of inflammatory markers (c) The BDEVs expressed small EV enriched markers and demonstrated an absence of small EV non-enriched markers ( $n = 3$ , two LPS TB samples and BDEVs, and one control TB sample and BDEV). (d) A population of vesicles with depressed cup-like structures and a diameter of 100 to 200 nm, consistent with that of small EVs, appear to be present in the TEM images. These images are representative of a control sample (left) and an LPS samples (right). (e) The BDEVs appear to be between 100 and 200 nm in diameter, consistent with small EVs, as shown by the nanoparticle tracking analysis. This result is representative of  $n = 3$  (one control BDEV sample and two LPS BDEV samples). BDEV, brain derived extracellular vesicles; LPS, lipopolysaccharide; TB, brain tissue; TEM, transmission electron microscopy.

modifications of oxidation of M, and acetylation and/or methionine loss of protein N-terminus. Validation FDR thresholds were 0.01 for strict or 0.05 for relaxed criteria at PSM, peptide and protein levels. Label-free quantification was performed on precursor ion intensity and abundances were normalised to total peptide amount. Possible contaminants were identified with the protein marker node and the Common Repository of Adventitious Peptides database.

## 2.10 | Statistical analysis and data availability

Proteome discoverer protein abundances were processed with Perseus (Tyanova et al., 2016), where contaminants were removed, values were log base 2 transformed, filtered to remove proteins that lacked three valid values in at least one treatment, and missing values were imputed (2 SD downshifted distribution and 0.2 SD width). Downstream analysis was performed using the DEP: Differential Enrichment analysis of Proteomics data package in R studio and differential analysis was conducted using the packages in-built software and recommended settings (Zhang et al., 2018). The resulting data were presented using GraphPad Prism where the volcano plots represent all of the proteins detected in the total brain samples and BDEVs with significant proteins being determined to have a fold change of  $\geq 1.5$  or  $\leq -1.5$  and a  $p$ -value of  $\leq 0.05$  (Version 8.2.1; GraphPad Software

Inc, San Diego, CA, USA). Downstream analysis included STRING analysis, gProfiler (performed on the 1 March 2022 for the BDEVs and the 2 March 2022 for the TBs), which were visually presented using Biorender, and the R package ggplot2: Elegant Graphics for Data Analysis, where the number of proteins involved in each GO category is represented by the length of the bar and the colour of the bar represents the  $-\log_{10}$  of the adjusted  $p$ -value for that category (Szklarczyk et al., 2015). The proteomics data has been submitted to the PRIDE repository and can be accessed using the identifier PXD044893. Pro-inflammatory mRNA data were analysed using GraphPad Prism (Version 8.2.1; GraphPad Software Inc, San Diego, CA, USA). Saline control and LPS-treated groups were compared using individual Student's  $t$ -tests or Mann–Whitney  $U$  tests for non-normally distributed data. All data were presented as the mean  $\pm$  standard error of the mean (SEM) and  $p < 0.05$  was considered statistically significant.

### 3 | RESULTS

#### 3.1 | LPS-induced neuroinflammation and BDEV characterisation

Using a panel of pro-inflammatory mRNA, the neuroinflammatory effects of LPS administration were evaluated in the cortical tissue from the treated mice. There were highly significant increases in expression of the chemokines, cytokines and inflammatory markers *Ccl2* ( $p < 0.05$ ), *Tnf* ( $p < 0.05$ ), *Il1 $\beta$*  ( $p < 0.001$ ), *Il6* ( $p < 0.001$ ), *Nlrp3* ( $p < 0.001$ ) and *Nfkb* ( $p < 0.001$ ) in LPS-treated mice relative to controls (Figures 1a and b). BDEVs and representative total brain tissue (TB) samples were isolated from the cortex of mice following treatment with LPS (500  $\mu\text{g}/\text{kg}$ ) ( $n = 3$  for BDEVs and  $n = 4$  for TB) or saline ( $n = 3$  for BDEVs and  $n = 4$  for TB) for 6 h. Quality control assessments were conducted to ensure the BDEVs met MISEV's minimum criteria to be classified as small EVs (Thery et al., 2018). This involved Western blot analysis, where the EVs were probed with EV enriched markers: Actin, Tsg101 and CD9 and non-EV enriched markers: calnexin and nucleoporin to ensure the presence of small EVs and the absence of contamination (Figure 1c). The EVs underwent TEM where they exhibited a homogenous vesicle population consisting of EVs with depressed cup-like structures and a size of 40–120 nm in diameter (Figure 1d) (Wu et al., 2015). This size was further verified through NTA analysis, performed on the ZetaView Quatt PMX-420 (Figure 1e) (Kalra et al., 2012; Sokolova et al., 2011). Following successful characterisation, the BDEVs underwent proteomic analysis.

#### 3.2 | Upregulated proteins were identified in the brain tissue and BDEVs from LPS treated mice

The proteome of the LPS-treated mouse derived brain tissue (Table S1) and BDEVs (Table S2) was compared to that of the control mice to determine whether certain proteins were differentially expressed under inflammatory conditions. Fourteen proteins were found to be significantly differentially expressed in the brain tissue of the LPS treated mice, with majority of these proteins exhibiting upregulation during the inflammatory condition (Figure 2a). Interestingly, these upregulated proteins include S100 calcium-binding protein A8 (S100A8) and A9 (S100A9), two potent regulators of the inflammatory response, known to be released from activated microglia (Blom et al., 2020; Wang et al., 2018). Furthermore, the BDEV proteomes isolated from the LPS-treated and control mice were compared to determine whether EV proteomes changed during inflammation. The mass spectrometry results identified 57 differentially expressed proteins with a clear upregulation of proteins being observed in the BDEVs isolated from the LPS-treated mice compared to the control mice (Figures 2b). These groups of differentially expressed

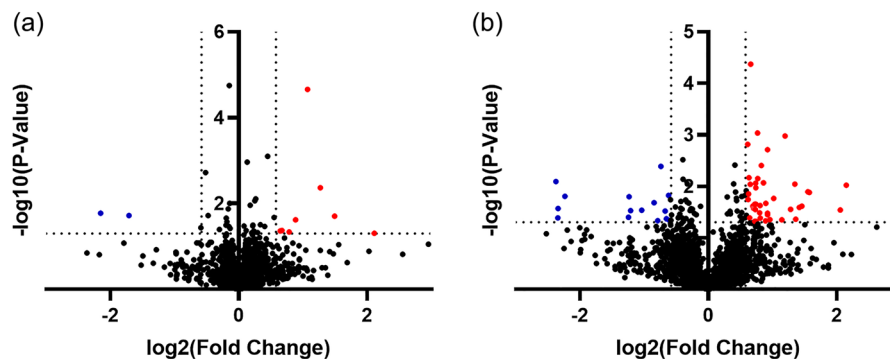
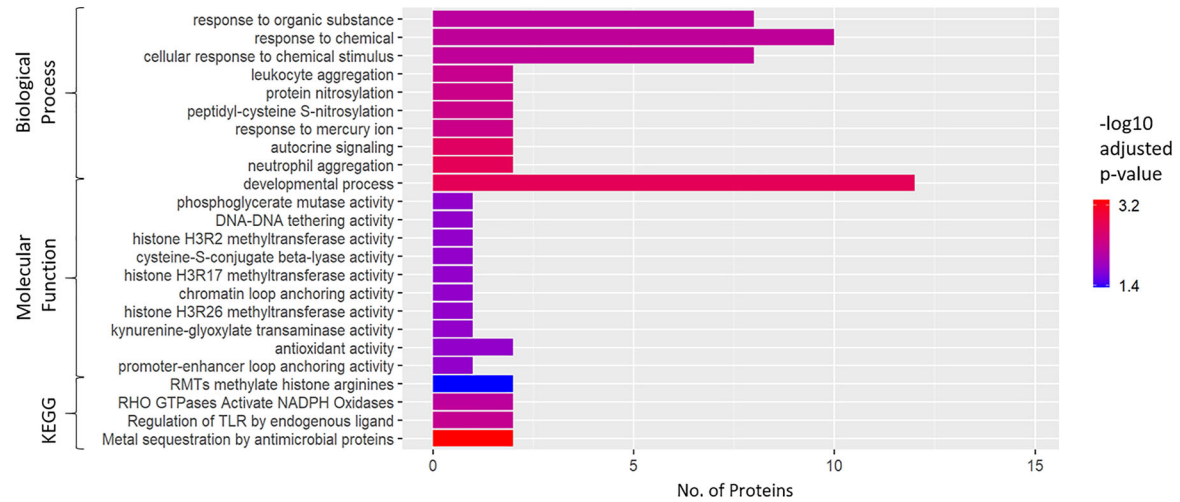


**FIGURE 2** Differentially expressed proteins observed in the TB and in the BDEVs from LPS treated mice compared to controls. (a) Fourteen proteins were found to be significantly differentially expressed in the TB of the LPS treated mice compared to the control mice. Log<sub>2</sub>(Fold Change) cut off of  $\pm 0.585$  and  $-\text{Log}_{10}(p\text{-value})$  cut off of 1.3. (b) 57 proteins were found to be significantly differentially expressed in the BDEVs isolated from the LPS treated mice compared to the control mice. Log<sub>2</sub>(Fold Change) cut off of  $\pm 0.585$  and  $-\text{Log}_{10}(p\text{-value})$  cut off of 1.3. BDEV, brain derived extracellular vesicles; LPS, lipopolysaccharide; TB, brain tissue.

(a) **Brain Tissue Gene Ontology**



(b) **Brain Derived Extracellular Vesicles Gene Ontology**

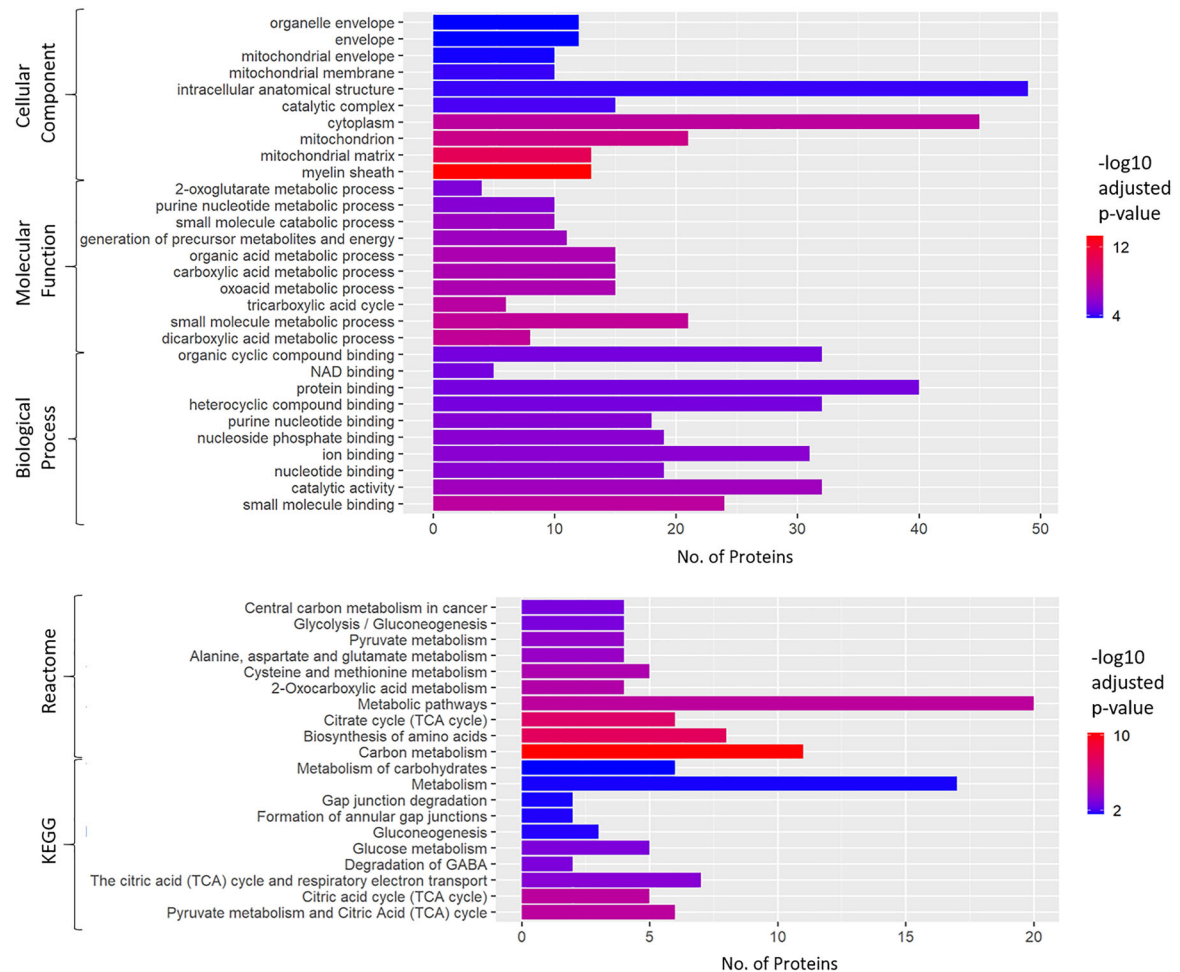


**FIGURE 3** GO analysis of the proteins found to be differentially expressed in the LPS treated mouse TB and BDEVs compared to the controls. GO analysis based on fold enrichment revealed the number of proteins involved in each category. The number of proteins involved in each GO category is represented by the length of the bar and the colour of the bar represents the  $-\log_{10}$  of the adjusted  $p$ -value for that category. (a) The differentially expressed TB proteins exhibited molecular functions including antioxidant and histone methyltransferase activity, and were involved in biological processes including the inflammatory response, neutrophil aggregation, and leukocyte migration. Finally, the proteins were found to be involved in regulation of TLR signalling as

(Continues)

**FIGURE 3** (Continued)

observed in the reactome pathway analysis. (b) The differentially expressed BDEV proteins were found to be involved in cellular components including the mitochondria and its membrane, exhibited molecular functions including NAD, and the TCA cycle, and were involved in biological processes including the metabolic processes and glycolysis. Finally, the proteins were found to be involved in regulation of TCA cycle, and platelet and degranulation as observed in the reactome pathway analysis. BDEV, brain derived extracellular vesicles; GO, Gene ontology; TB, brain tissue; TCA, tricarboxylic acid; TLR, toll-like receptor.

proteins were further examined through gene ontology (GO) analysis to determine which pathway were being affected through EV facilitation under inflammatory conditions.

### 3.3 | Upregulated proteins in the brain tissue of LPS treated mice execute the inflammatory response through immune cell activation and cysteine S-nitrosylation

GO analysis revealed the differentially expressed proteins in the brain tissue samples to be involved in clearance pathways and exhibited molecular functions including antioxidant activity (Figure 3a). Furthermore, these proteins were found to be involved in biological processes including peptidyl cysteine S-nitrosylation, neutrophil aggregation and leukocyte migration involved in the inflammatory response. Interestingly, the regulation of TLR by endogenous ligands appeared to be one of the reactome pathways determined to involve the proteins. Given the brain tissue appeared to exhibit an inflammatory response it was of interest to determine whether the activation of these pathways was being mediated through EVs.

### 3.4 | BDEV proteins from LPS treated mice are involved in key metabolic pathways

BDEV proteins isolated from the cortex of LPS treated and control mice were revealed, through GO analysis, to be associated with the mitochondria and mitochondrial matrix (Figure 3b). These proteins were found to exhibit molecular functions including NAD binding and carboxylic acid binding, functions that are synonymous with the mitochondria. Furthermore, these proteins were found to be involved in biological processes including the TCA cycle, 2-oxoglutarate metabolism and the NADH metabolic process. Additionally, through reactome analysis, these proteins were implicated in gluconeogenesis and glycolysis. Given, the GO results revealed an overwhelming proportion of proteins were involved in metabolic processes occurring in the mitochondria, STRING analysis was performed to determine whether any of the differentially expressed proteins were interacting partners. Interestingly, no network connectivity was identified between the proteins found to be differentially expressed in the brain tissue. Furthermore, only two interacting pairs were identified with one pair being the S100A8 and S100A9 proteins (Figure 4a). Contrastingly, STRING analysis revealed the differentially expressed proteins identified in the BDEVs isolated from the LPS-treated mice exhibited a significant network connectivity process (Figure 4b). Further investigation of this network revealed it consisted primarily of the upregulated proteins which were discovered to be enzymes involved in the TCA cycle or enzymes whose products fed into the TCA cycle in addition to, a component of the electron transport chain (Figure 5 and Table S3). The differentially expressed proteins found in the BDEVs were then investigated to determine whether they were originating from a specific cell type in the CNS. Proteins differentially expressed in the brain tissue samples and BDEVs appeared to be equally expressed across the CNS cell types with a slight enrichment of several proteins observed in the neuronal cells and enrichment of S100A8 and S100A9 in the macrophage progenitor cells (Figure S1). These pathway analysis results indicate the differentially expressed proteins are involved in the inflammatory response, and those packaged into EVs are involved in important network connectivity processes related to metabolic pathways occurring in the mitochondria that are predominantly occurring in neuronal and microglial cells during inflammation.

## 4 | DISCUSSION

To understand the role EVs play in acute neuroinflammatory conditions, this study isolated BDEVs from mice treated with LPS (500 µg/kg). Following EV isolation and characterisation, the samples underwent proteomic analysis where a panel of 14 differentially expressed proteins was identified in the brain tissue samples and a panel of 57 differentially expressed proteins was discovered in the BDEVs. The proteins differentially expressed in the LPS-treated mouse brain tissues encompassed known inflammatory molecules including low levels of alarmins, S100A8 and S100A9 (Blom et al., 2020; Wang et al., 2018). Alternatively, the upregulated proteins identified in BDEVs from LPS treated mice exhibited network relationships that suggested involvement with the TCA cycle, linking small EV packaging with the metabolic changes known to be associated with microglial and macrophage pro-inflammatory activation.

A panel of pro-inflammatory mRNA markers showed there was significant induction of neuroinflammation following 6 h of LPS treatment. This is largely in agreement with previous studies using LPS as a model of neuroinflammation (Biesmans



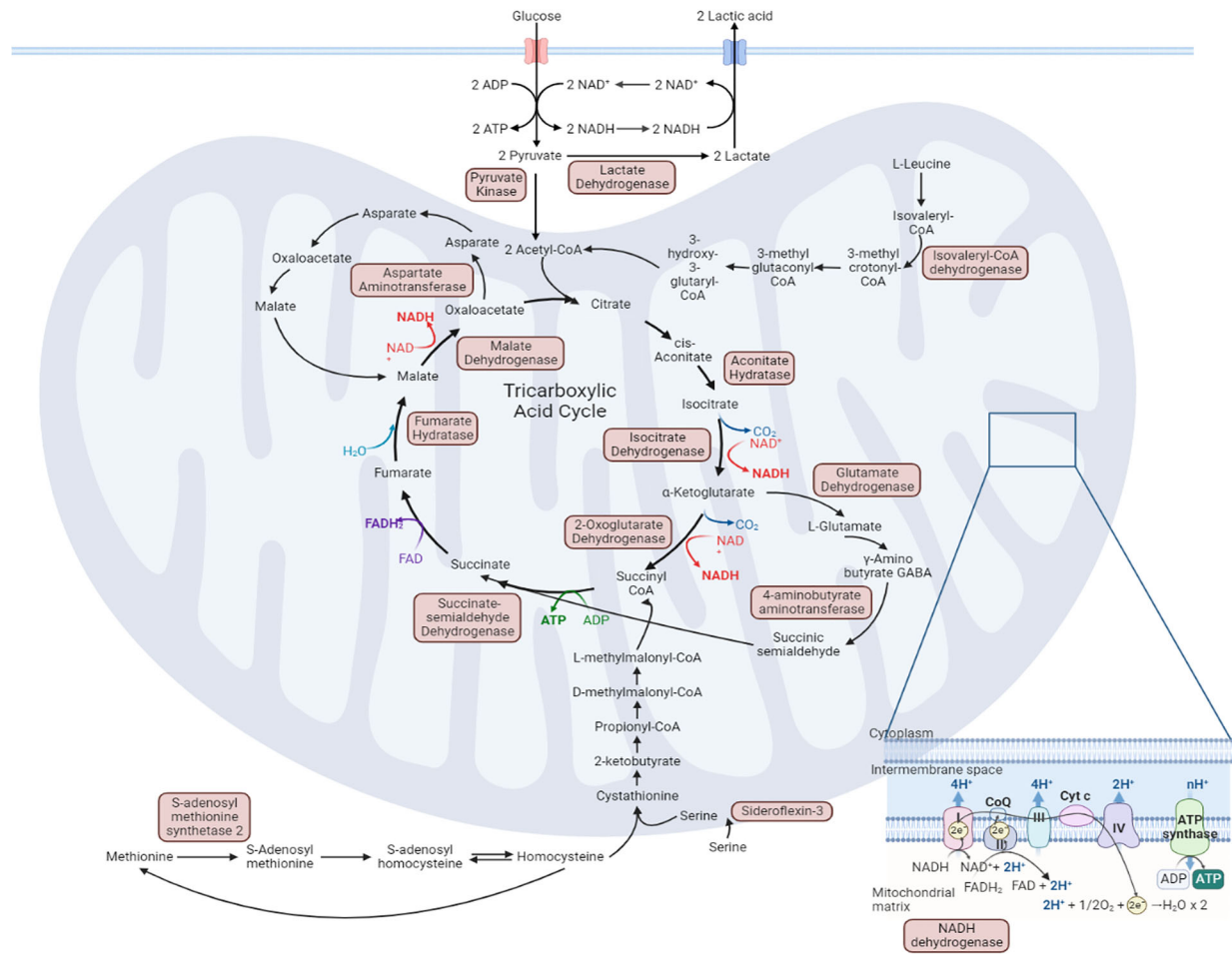


**FIGURE 5** The upregulated BDEVs proteins, isolated from the LPS treated mice, appear to be involved in the TCA cycle. Proteins identified to be enriched in the LPS-treated mouse BDEVs were found to constitute TCA cycle enzymes. Additionally, several of these proteins were found to comprise enzymes whose products feed into the TCA cycle and one of these proteins was found to form an electron transport chain protein complex, as indicated by the red boxes. BDEV, brain derived extracellular vesicles; LPS, lipopolysaccharide; TCA, tricarboxylic acid cycle.

et al., 2013; Dang et al., 2019; Mittli, 2023). Unsurprisingly, proteomic analysis of the LPS-treated mouse brain tissues revealed numerous proteins involved in initiating the inflammatory cascade and generation of ROS which are known to alter cellular communication. Therefore, examination of the BDEVs was conducted next to determine whether this is reflected in the released EVs.

Several downregulated proteins were identified in the BDEVs derived from the LPS treated mice compared to the controls. These proteins included calcium/calmodulin-dependent protein kinase type II (CaMKII), a prominent player in glutamatergic synaptic plasticity. Increased phosphorylation and expression of CaMKII is induced through LPS treatment resulting in the formation of N-methyl D-aspartate receptor subtype 2B-CaMKII-Postsynaptic density protein 95 in the frontal cortex and hippocampus of mice where the proteins' presence is associated with neuronal damage (Song et al., 2019). In addition to mediating inflammation, CaMKII is known to be involved in apoptotic pathways and its increased phosphorylation and expression has been observed in mouse brain tissues undergoing necroptosis after intracerebral haemorrhage (Sun et al., 2023; Yuan et al., 2023).

Examination of the upregulated proteins in the BDEVs derived from the LPS treated mice revealed a network connectivity map indicating a high degree of interaction. Upon further examination, these proteins were all found to be a part of, or feed into the TCA cycle. In previous studies, LPS was shown to induce macrophages to preferentially undergo glycolysis as opposed to oxidative phosphorylation, diminishing TCA cycle activity (Choi et al., 2021; Haas et al., 2016; Tannahill et al., 2013). The downregulation of isocitrate dehydrogenase in macrophages is believed to assist their polarization into the pro-inflammatory phenotype, (Jha et al., 2015; Liu et al., 2017). Interestingly,  $\alpha$ -ketoglutarate dehydrogenase levels are known to decrease upon LPS stimulation (Ji et al., 2020). Furthermore, succinate promotes HIF-1 $\alpha$  stabilization and IL-1 $\beta$  generation by post-transcriptionally modifying enzymes including malate dehydrogenase, whose metabolic process was one of the affected biological functions, and pyruvate kinase which enhances macrophage pro-inflammatory activity, an affect that is ameliorated by  $\alpha$ -ketoglutarate (Liu et al., 2016; Mills et al., 2016; Tannahill et al., 2013; Zhang et al., 2011). Interestingly, LPS-induced STAT1 activity promotes autophagy through TLR4 activation, inducing a pro-inflammatory state in primary murine and rat microglia (Hu et al., 2021; Qin et al., 2018).

Similarly, peptidoglycan-stimulation of cultured murine microglia leads to TLR2 activation resulting in autophagic upregulation and an inflammatory state (Ma et al., 2020). This pro-inflammatory state is abolished either through anti-inflammatory drugs or autophagic inhibitors (Hu et al., 2021; Qin et al., 2018). Given the overlap between autophagy and EV biogenesis, this may be a potential pathway that promotes packaging of TCA cycle components into EVs to prevent impeding the increased autophagic flux. It should be noted that the BDEVs used in this study were isolated from frozen cortical tissue. Although we did not see any indication cellular degradation via nuclear bodies or endoplasmic reticulum vesicles with nucleoporin or calnexin examination respectively, other factors may be released which could contribute to the results seen here. However, other studies using snap frozen mouse brain tissue have highlighted BDEVs can be successfully isolated from snap frozen mouse, macaque monkey and human tissues for RNA sequencing and proteomics using the same process we have utilised here (Huang et al., 2020; Vassileff, Vella, Rajapaksha, et al., 2020).

This study identified 14 differentially expressed proteins in the LPS brain tissue samples and 57 in the BDEVs derived from the LPS brain tissue samples, suggesting EV packaging is highly regulated early in inflammation. Several proteins identified in the BDEVs have previously been associated with initiating the inflammatory response. Additionally, proteins involved in epigenetic regulation were also differentially regulated in both the BDEVs and brain tissue isolated from the LPS-treated mice compared to the controls. Together, these results link early pro-inflammatory activation with small EV cargo packaging and indicate this may be substantially regulated in acute inflammation. Further studies should confirm the link between metabolism and EV packaging, ideally identifying cell types modulating cellular communication during early inflammation.

## AUTHOR CONTRIBUTIONS

**Natasha Vassileff:** Conceptualization (equal); data curation (equal); formal analysis (equal); investigation (equal); writing—original draft (equal). **Jereme G. Spiers:** Conceptualization (equal); data curation (equal); formal analysis (equal); investigation (equal); writing—original draft (equal). **Juliani Juliani:** Data curation (supporting); formal analysis (supporting). **Rohan G. T. Lowe:** Formal analysis (supporting); writing—review and editing (supporting). **Keshava K. Datta:** Formal analysis (supporting); writing—review and editing (supporting). **Andrew F. Hill:** Conceptualization (supporting); methodology (supporting); resources (lead); supervision (equal); writing—review and editing (supporting).

## ACKNOWLEDGEMENTS

Jereme G. Spiers is supported by a Royce Simmons Foundation Mid-Career Research Fellowship through the Dementia Australia Research Foundation. We would also like to acknowledge the La Trobe University Bioimaging Platform for microscopy support, and the La Trobe University Proteomics and Metabolomics Platform for proteomics support. This work was supported by the National Health and Medical Research Council Australia under Grant [GNT1132604]. The funding bodies had no further role in the study design; in the collection, analysis, and interpretation of data; in the writing of the report; and in the decision to submit the paper for publication.

Open access publishing facilitated by Victoria University, as part of the Wiley - Victoria University agreement via the Council of Australian University Librarians.

## CONFLICT OF INTEREST STATEMENT

The authors declare no conflicts of interest.

## ORCID

Natasha Vassileff  <https://orcid.org/0000-0001-6554-4496>

Jereme G. Spiers  <https://orcid.org/0000-0001-5872-8983>

Andrew F. Hill  <https://orcid.org/0000-0001-5581-2354>

## REFERENCES

- Batista, C. R. A., Gomes, G. F., Candelario-Jalil, E., Fiebich, B. L., & de Oliveira, A. C. P. (2019). Lipopolysaccharide-induced neuroinflammation as a bridge to understand neurodegeneration. *International Journal of Molecular Sciences*, 20(9), 2293.
- Biesmans, S., Meert, T. F., Bouwknecht, J. A., Acton, P. D., Davoodi, N., De Haes, P., Kuijlaars, J., Langlois, X., Matthews, L. J., Ver Donck, L., Hellings, N., & Nuydens, R. (2013). Systemic immune activation leads to neuroinflammation and sickness behavior in mice. *Mediators of Inflammation*, 2013, 271359.
- Blom, A. B., van den Bosch, M. H., Blaney Davidson, E. N., Roth, J., Vogl, T., van de Loo, F. A., Koenders, M., van der Kraan, P. M., Geven, E. J., & van Lent, P. L. (2020). The alarmins S100A8 and S100A9 mediate acute pain in experimental synovitis. *Arthritis Research & Therapy*, 22, 199.
- Buschow, S. I., Nolte-<sup>t</sup>Hoen, E. N., van Niel, G., Pols, M. S., ten Broeke, T., Lauwen, M., Ossendorp, F., Melief, C. J., Raposo, G., Wubbolts, R., Wauben, M. H., & Stoorvogel, W. (2009). MHC II in dendritic cells is targeted to lysosomes or T cell-induced exosomes via distinct multivesicular body pathways. *Traffic*, 10, 1528–1542.
- Choi, I., Son, H., & Baek, J. H. (2021). Tricarboxylic acid (TCA) cycle intermediates: Regulators of immune responses. *Life*, 11(1), 69.
- Colletti, M., Ceglie, D., Di Giannatale, A., & Nazio, F. (2021). Autophagy and exosomes relationship in cancer: Friends or foes? *Frontiers in Cell and Developmental Biology*, 8, 614178.
- Dang, R., Guo, Y.-y., Zhang, K., Jiang, P., & Zhao, M.-g (2019). Predictable chronic mild stress promotes recovery from LPS-induced depression. *Molecular Brain*, 12, 42.
- DiSabato, D. J., Quan, N., & Godbout, J. P. (2016). Neuroinflammation: The devil is in the details. *Journal of Neurochemistry*, 139(Suppl 2), 136–153.

- Fader, C. M., Sánchez, D., Furlán, M., & Colombo, M. I. (2008). Induction of autophagy promotes fusion of multivesicular bodies with autophagic vacuoles in k562 cells. *Traffic*, *9*, 230–250.
- Ge, Y., Huang, M., & Yao, Y. M. (2018). Autophagy and proinflammatory cytokines: Interactions and clinical implications. *Cytokine & Growth Factor Reviews*, *43*, 38–46.
- Geiß, C., Salas, E., Guevara-Coto, J., Régnier-Vigouroux, A., & Mora-Rodríguez, R. A. (2022). Multistability in Macrophage Activation Pathways and Metabolic Implications. *Cells*, *11*(3), 404.
- Glick, D., Barth, S., & Macleod, K. F. (2010). Autophagy: Cellular and molecular mechanisms. *Journal of Pathology*, *221*, 3–12.
- Gudbergsson, J. M., & Johnsen, K. B. (2019). Exosomes and autophagy: Rekindling the vesicular waste hypothesis. *Journal of Cell Communication and Signaling*, *13*, 443–450.
- Guo, H., Chitiprolu, M., Roncevic, L., Javalet, C., Hemming, F. J., Trung, M. T., Meng, L., Latreille, E., Tanese de Souza, C., McCulloch, D., Baldwin, R. M., Auer, R., Côté, J., Russell, R. C., Sadoul, R., & Gibbins, D. (2017). Atg5 disassociates the V(1)V(0)-ATPase to promote exosome production and tumor metastasis independent of canonical macroautophagy. *Developmental Cell*, *43*, 716–730.e7.
- Haas, R., Cucchi, D., Smith, J., Pucino, V., Macdougall, C. E., & Mauro, C. (2016). Intermediates of metabolism: From bystanders to signalling molecules. *Trends in Biochemical Sciences*, *41*, 460–471.
- Hu, L., Yu, Y., Huang, H., Fan, H., Hu, L., Yin, C., Li, K., Fulton, D. J., & Chen, F. (2016). Epigenetic regulation of interleukin 6 by histone acetylation in macrophages and its role in paraquat-induced pulmonary fibrosis. *Frontiers in Immunology*, *7*, 696.
- Hu, Z. W., Zhou, L. Q., Yang, S., Chen, M., Yu, H. H., Tao, R., Wu, L. J., Wang, W., Zhang, Q., Qin, C., & Tian, D. S. (2021). FTY720 modulates microglia toward anti-inflammatory phenotype by suppressing autophagy via STAT1 pathway. *Cellular and Molecular Neurobiology*, *41*, 353–364.
- Huang, Y., Cheng, L., Turchinovich, A., Mahairaki, V., Troncoso, J. C., Pletniková, O., Haughey, N. J., Vella, L. J., Hill, A. F., Zheng, L., & Witwer, K. W. (2020). Influence of species and processing parameters on recovery and content of brain tissue-derived extracellular vesicles. *Journal of Extracellular Vesicles*, *9*, 1785746.
- Jha, A. K., Huang, S. C., Sergushichev, A., Lampropoulou, V., Ivanova, Y., Loginicheva, E., Chmielewski, K., Stewart, K. M., Ashall, J., Everts, B., Pearce, E. J., Driggers, E. M., & Artyomov, M. N. (2015). Network integration of parallel metabolic and transcriptional data reveals metabolic modules that regulate macrophage polarization. *Immunity*, *42*, 419–430.
- Ji, D., Yin, J. Y., Li, D. F., Zhu, C. T., Ye, J. P., & Pan, Y. Q. (2020). Effects of inflammatory and anti-inflammatory environments on the macrophage mitochondrial function. *Scientific Reports*, *10*, 20324.
- Kalra, H., Simpson, R. J., Ji, H., Aikawa, E., Altevogt, P., Askenase, P., Bond, V. C., Borràs, F. E., Breakefield, X., Budnik, V., Buzas, E., Camussi, G., Clayton, A., Cocucci, E., Falcon-Perez, J. M., Gabrielson, S., Ghossein, Y. S., Gupta, D., Harsha, H. C., ... Mathivanan, S. (2012). Vesiclepedia: A compendium for extracellular vesicles with continuous community annotation. *PLoS Biology*, *10*, e1001450.
- Kim, J. W., Tchernyshyov, I., Semenza, G. L., & Dang, C. V. (2006). HIF-1-mediated expression of pyruvate dehydrogenase kinase: A metabolic switch required for cellular adaptation to hypoxia. *Cell Metabolism*, *3*, 177–185.
- Kowal, J., Arras, G., Colombo, M., Jouve, M., Morath, J. P., Primdal-Bengtson, B., Dingli, F., Loew, D., Tkach, M., & Théry, C. (2016). Proteomic comparison defines novel markers to characterize heterogeneous populations of extracellular vesicle subtypes. *PNAS*, *113*, E968–E977.
- Lauterbach, M. A., Hanke, J. E., Serefidou, M., Mangan, M. S. J., Kolbe, C. C., Hess, T., Rothe, M., Kaiser, R., Hoss, F., Gehlen, J., Engels, G., Kreutzenbeck, M., Schmidt, S. V., Christ, A., Imhof, A., Hiller, K., & Latz, E. (2019). Toll-like receptor signaling rewires macrophage metabolism and promotes histone acetylation via ATP-citrate lyase. *Immunity*, *51*, 997–1011.e7.
- Lu, Y. C., Yeh, W. C., & Ohashi, P. S. (2008). LPS/TLR4 signal transduction pathway. *Cytokine*, *42*, 145–151.
- Liu, L., Lu, Y., Martinez, J., Bi, Y., Lian, G., Wang, T., Milasta, S., Wang, J., Yang, M., Liu, G., Green, D. R., & Wang, R. (2016). Proinflammatory signal suppresses proliferation and shifts macrophage metabolism from Myc-dependent to HIF1 $\alpha$ -dependent. *Proceedings of the National Academy of Sciences of the United States of America*, *113*, 1564–1569.
- Liu, P. S., Wang, H., Li, X., Chao, T., Teav, T., Christen, S., Di Conza, G., Cheng, W. C., Chou, C. H., Vavakova, M., Muret, C., Debackere, K., Mazzone, M., Huang, H. D., Fendt, S. M., Ivanisevic, J., & Ho, P. C. (2017).  $\alpha$ -ketoglutarate orchestrates macrophage activation through metabolic and epigenetic reprogramming. *Nature Immunology*, *18*, 985–994.
- Ma, K., Guo, J., Wang, G., Ni, Q., & Liu, X. (2020). Toll-like receptor 2-mediated autophagy promotes microglial cell death by modulating the microglial M1/M2 phenotype. *Inflammation*, *43*, 701–711.
- Meiser, J., Krämer, L., Sapcariu, S. C., Battello, N., Ghelfi, J., D’Herouel, A. F., Skupin, A., & Hiller, K. (2016). Pro-inflammatory macrophages sustain pyruvate oxidation through pyruvate dehydrogenase for the synthesis of itaconate and to enable cytokine expression. *The Journal of Biological Chemistry*, *291*, 3932–3946.
- Mills, E. L., Kelly, B., Logan, A., Costa, A. S. H., Varma, M., Bryant, C. E., Toulomousis, P., Däbritz, J. H. M., Gottlieb, E., Latorre, I., Corr, S. C., McManus, G., Ryan, D., Jacobs, H. T., Szibor, M., Xavier, R. J., Braun, T., Frezza, C., Murphy, M. P., & O’Neill, L. A. (2016). Succinate dehydrogenase supports metabolic repurposing of mitochondria to drive inflammatory macrophages. *Cell*, *167*, 457–470.e13.
- Mittli, D. (2023). Inflammatory processes in the prefrontal cortex induced by systemic immune challenge: Focusing on neurons. *Brain, Behavior, & Immunity—Health*, *34*, 100703.
- Murrow, L., Malhotra, R., & Debnath, J. (2015). ATG12-ATG3 interacts with Alix to promote basal autophagic flux and late endosome function. *Nature Cell Biology*, *17*, 300–310.
- Norden, D. M., Trojanowski, P. J., Villanueva, E., Navarro, E., & Godbout, J. P. (2016). Sequential activation of microglia and astrocyte cytokine expression precedes increased Iba-1 or GFAP immunoreactivity following systemic immune challenge. *Glia*, *64*, 300–316.
- Pan, B. T., Teng, K., Wu, C., Adam, M., & Johnstone, R. M. (1985). Electron microscopic evidence for externalization of the transferrin receptor in vesicular form in sheep reticulocytes. *The Journal of Cell Biology*, *101*, 942–948.
- Perez-Hernandez, J., Olivares, D., Forner, M. J., Ortega, A., Solaz, E., Martinez, F., Chaves, F. J., Redon, J., & Cortes, R. (2018). Urinary exosome miR-146a is a potential marker of albuminuria in essential hypertension. *Journal of Translational Medicine*, *16*, 228.
- Qin, C., Liu, Q., Hu, Z. W., Zhou, L. Q., Shang, K., Bosco, D. B., Wu, L. J., Tian, D. S., & Wang, W. (2018). Microglial TLR4-dependent autophagy induces ischemic white matter damage via STAT1/6 pathway. *Theranostics*, *8*, 5434–5451.
- Rappilber, J., Mann, M., & Ishihama, Y. (2007). Protocol for micro-purification, enrichment, pre-fractionation and storage of peptides for proteomics using StageTips. *Nature Protocols*, *2*, 1896–1906.
- Sanosaka, M., Fujimoto, M., Ohkawara, T., Nagatake, T., Itoh, Y., Kagawa, M., Kumagai, A., Fuchino, H., Kunisawa, J., Naka, T., & Takemori, H. (2015). Salt-inducible kinase 3 deficiency exacerbates lipopolysaccharide-induced endotoxin shock accompanied by increased levels of pro-inflammatory molecules in mice. *Immunology*, *145*, 268–278.

- Shi, B., Huang, Q., Tak, P. P., Vervoordeldonk, M. J., Huang, C. C., Dorfleutner, A., Stehlik, C., & Pope, R. M. (2012). SNAPIN: An endogenous Toll-like receptor ligand in rheumatoid arthritis. *Annals of the Rheumatic Diseases*, *71*, 1411–1417.
- Skotland, T., Sandvig, K., & Llorente, A. (2017). Lipids in exosomes: Current knowledge and the way forward. *Progress in Lipid Research*, *66*, 30–41.
- Sokolova, V., Ludwig, A. K., Hornung, S., Rotan, O., Horn, P. A., Epple, M., & Giebel, B. (2011). Characterisation of exosomes derived from human cells by nanoparticle tracking analysis and scanning electron microscopy. *Colloids and Surfaces B: Biointerfaces*, *87*, 146–150.
- Song, Y., Zhao, X., Wang, D., Zheng, Y., Dai, C., Guo, M., Qin, L., Wen, X., Zhou, X., & Liu, Z. (2019). Inhibition of LPS-induced brain injury by NR2B antagonists through reducing assembly of NR2B-CaMKII-PSD95 signal module. *Immunopharmacology and Immunotoxicology*, *41*, 86–94.
- Stoorvogel, W., Strous, G. J., Geuze, H. J., Oorschot, V., & Schwartz, A. L. (1991). Late endosomes derive from early endosomes by maturation. *Cell*, *65*, 417–427.
- Sun, T., Tan, L., Liu, M., Zeng, L., Zhao, K., Cai, Z., Sun, S., Li, Z., & Liu, R. (2023). Tiliain improves cognition in a vascular dementia rodent model by targeting miR-193b-3p/CaM- and miR-152-3p/CaMKII $\alpha$ -mediated inflammatory and apoptotic pathways. *Frontiers in Immunology*, *14*, 1118808.
- Szklarczyk, D., Franceschini, A., Wyder, S., Forslund, K., Heller, D., Huerta-Cepas, J., Simonovic, M., Roth, A., Santos, A., Tsafou, K. P., Kuhn, M., Bork, P., Jensen, L. J., & von Mering, C. (2015). STRING v10: Protein-protein interaction networks, integrated over the tree of life. *Nucleic Acids Research*, *43*, D447–D452.
- Tannahill, G. M., Curtis, A. M., Adamik, J., Palsson-McDermott, E. M., McGettrick, A. F., Goel, G., Frezza, C., Bernard, N. J., Kelly, B., Foley, N. H., Zheng, L., Gardet, A., Tong, Z., Jany, S. S., Corr, S. C., Haneklaus, M., Caffrey, B. E., Pierce, K., Walmsley, S., ... O'Neill, L. A. (2013). Succinate is an inflammatory signal that induces IL-1 $\beta$  through HIF-1 $\alpha$ . *Nature*, *496*, 238–242.
- Thery, C., Witwer, K. W., Aikawa, E., Alcaraz, M. J., Anderson, J. D., Andriantsitohaina, R., Antoniou, A., Arab, T., Archer, F., Atkin-Smith, G. K., Ayre, D. C., Bach, J. M., Bachurski, D., Baharvand, H., Balaj, L., Baldacchino, S., Bauer, N. N., Baxter, A. A., Bebawy, M., ... Zuba-Surma, E. K. (2018). Minimal information for studies of extracellular vesicles 2018 (MISEV2018): A position statement of the International Society for Extracellular Vesicles and update of the MISEV2014 guidelines. *Journal of Extracellular Vesicles*, *7*, 1535750.
- Tyanova, S., Temu, T., Sinitcyn, P., Carlson, A., Hein, M. Y., Geiger, T., Mann, M., & Cox, J. (2016). The Perseus computational platform for comprehensive analysis of (prote)omics data. *Nature Methods*, *13*, 731–740.
- Vassileff, N., Cheng, L., & Hill, A. F. (2020). Extracellular vesicles—Propagators of neuropathology and sources of potential biomarkers and therapeutics for neurodegenerative diseases. *Journal of Cell Science*, *133*(23), jcs243139.
- Vassileff, N., Vella, L. J., Rajapaksha, H., Shambrook, M., Kenari, A. N., McLean, C., Hill, A. F., & Cheng, L. (2020). Revealing the proteome of motor cortex derived extracellular vesicles isolated from amyotrophic lateral sclerosis human postmortem tissues. *Cells*, *9*(7), 1709.
- Vella, L. J., Scicluna, B. J., Cheng, L., Bawden, E. G., Masters, C. L., Ang, C. S., Williamson, N., McLean, C., Barnham, K. J., & Hill, A. F. (2017). A rigorous method to enrich for exosomes from brain tissue. *Journal of Extracellular Vesicles*, *6*, 1348885.
- Vicencio, E., Beltrán, S., Labrador, L., Manque, P., Nassif, M., & Woehlbier, U. (2020). Implications of selective autophagy dysfunction for ALS pathology. *Cells*, *9*, 381.
- Villarroya-Beltri, C., Baixauli, F., Mittelbrunn, M., Fernández-Delgado, I., Torralba, D., Moreno-Gonzalo, O., Baldanta, S., Enrich, C., Guerra, S., & Sánchez-Madrid, F. (2016). ISGylation controls exosome secretion by promoting lysosomal degradation of MVB proteins. *Nature Communications*, *7*, 13588.
- Wang, B., Rao, Y. H., Inoue, M., Hao, R., Lai, C. H., Chen, D., McDonald, S. L., Choi, M. C., Wang, Q., Shinohara, M. L., & Yao, T. P. (2014). Microtubule acetylation amplifies p38 kinase signalling and anti-inflammatory IL-10 production. *Nature Communications*, *5*, 3479.
- Wang, T., Liu, H., Lian, G., Zhang, S. Y., Wang, X., & Jiang, C. (2017). HIF1 $\alpha$ -induced glycolysis metabolism is essential to the activation of inflammatory macrophages. *Mediators of Inflammation*, *2017*, 9029327.
- Wang, S., Song, R., Wang, Z., Jing, Z., Wang, S., & Ma, J. (2018). S100A8/A9 in inflammation. *Frontiers in Immunology*, *9*, 1298.
- Wang, L., Klionsky, D. J., & Shen, H. M. (2022). The emerging mechanisms and functions of microautophagy. *Nature Reviews Molecular Cell Biology*, *24*(3), 186–203.
- Wculek, S. K., Dunphy, G., Heras-Murillo, I., Mastrangelo, A., & Sancho, D. (2022). Metabolism of tissue macrophages in homeostasis and pathology. *Cellular & Molecular Immunology*, *19*, 384–408.
- Wei, X., Song, H., Yin, L., Rizzo, M. G., Sidhu, R., Covey, D. F., Ory, D. S., & Semenkovich, C. F. (2016). Fatty acid synthesis configures the plasma membrane for inflammation in diabetes. *Nature*, *539*, 294–298.
- Wellen, K. E., Hatzivassiliou, G., Sachdeva, U. M., Bui, T. V., Cross, J. R., & Thompson, C. B. (2009). ATP-citrate lyase links cellular metabolism to histone acetylation. *Science*, *324*, 1076–1080.
- Wu, Y., Deng, W., & Klinke, D. J. (2015). Exosomes: Improved methods to characterize their morphology, RNA content, and surface protein biomarkers. *The Analyst*, *140*, 6631–6642.
- Yuan, G., Cao, C., Cao, D., Li, B., Li, X., Li, H., Shen, H., Wang, Z., & Chen, G. (2023). Receptor-interacting protein 3-phosphorylated Ca(2+) /calmodulin-dependent protein kinase II and mixed lineage kinase domain-like protein mediate intracerebral hemorrhage-induced neuronal necroptosis. *Journal of Neurochemistry*, *164*, 94–114.
- Zhang, Z., Tan, M., Xie, Z., Dai, L., Chen, Y., & Zhao, Y. (2011). Identification of lysine succinylation as a new post-translational modification. *Nature Chemical Biology*, *7*, 58–63.
- Zhang, X., Smits, A. H., van Tilburg, G. B. A., Ovaa, H., Huber, W., & Vermeulen, M. (2018). Proteome-wide identification of ubiquitin interactions using UbIA-MS. *Nature Protocols*, *13*, 530–550.
- Zhao, J., Bi, W., Xiao, S., Lan, X., Cheng, X., Zhang, J., Lu, D., Wei, W., Wang, Y., Li, H., Fu, Y., & Zhu, L. (2019). Neuroinflammation induced by lipopolysaccharide causes cognitive impairment in mice. *Scientific Reports*, *9*, 5790.

## SUPPORTING INFORMATION

Additional supporting information can be found online in the Supporting Information section at the end of this article.

**How to cite this article:** Vassileff, N., Spiers, J. G., Juliani, J., Lowe, R. G. T., Datta, K. K., & Hill, A. F. (2024). Acute neuroinflammation promotes a metabolic shift that alters extracellular vesicle cargo in the mouse brain cortex. *Journal of Extracellular Biology*, *3*, e165. <https://doi.org/10.1002/jex2.165>